

1998

Higher Order Isotropic Velocity Grids in Lattice Methods

Pavol Pavlo

George Vahala

Linda L. Vahala

Old Dominion University, lvahala@odu.edu

Follow this and additional works at: https://digitalcommons.odu.edu/ece_fac_pubs



Part of the [Physics Commons](#)

Repository Citation

Pavlo, Pavol; Vahala, George; and Vahala, Linda L., "Higher Order Isotropic Velocity Grids in Lattice Methods" (1998). *Electrical & Computer Engineering Faculty Publications*. 55.

https://digitalcommons.odu.edu/ece_fac_pubs/55

Original Publication Citation

Pavlo, P., Vahala, G., & Vahala, L. (1998). Higher order isotropic velocity grids in lattice methods. *Physical Review Letters*, 80(18), 3960-3963. doi: 10.1103/PhysRevLett.80.3960

Higher Order Isotropic Velocity Grids in Lattice Methods

Pavol Pavlo

Institute of Plasma Physics, Czech Academy of Sciences, Praha 8, Czech Republic

George Vahala*

Department of Physics, College of William & Mary, Williamsburg, Virginia 23187

Linda Vahala

Department of Electrical & Computer Engineering, Old Dominion University, Norfolk, Virginia 23529

(Received 8 December 1997)

Kinetic lattice methods are a very attractive representation of nonlinear macroscopic systems because of their inherent parallelizability on multiple processors and their avoidance of the nonlinear convective terms. By uncoupling the velocity lattice from the spatial grid, one can employ higher order (non-space-filling) isotropic lattices—lattices which greatly enhance the stable parameter regions, particularly in thermal problems. In particular, the superiority of the octagonal lattice over previous models used in 2D (hexagonal or square) and 3D (projected face-centered hypercube) is shown. [S0031-9007(98)05978-X]

PACS numbers: 47.11.+j, 05.50.+q

Lattice methods can play a major role in solving systems, particularly those whose evolution involves nonlinear advection terms. In particular, the kinetic lattice gas [1] and lattice Boltzmann [2] methods have been implemented successfully in the solution of Navier-Stokes flows, magnetohydrodynamics, flow through porous media, turbulent flows, phase transitions, multiphase flows, and chemically reacting flows as well as to liquid crystals and semiclassical transport in semiconductors. In many instances, lattice methods can be viewed as a maximally discretized molecular dynamics—an optimized mesoscopic description between the full molecular dynamics and the macroscopic conservation laws. However, nearly all applications have been restricted to macroscopic systems that are closed below the second moment (energy) level. Only a few attempts [3–6] have been successful in simulating thermal lattice Boltzmann systems (TLBE) because inherent numerical instabilities severely limit the accessible parameter regimes [5]. It is the purpose of this Letter to suggest a new TLBE model that displays numerical stability over a wide range of parameters—not only in 2D, but also in 3D.

In their simplest form, these kinetic lattice models are ideally implemented on multiparallel processors because all operations are purely local; the Lagrangian schemes are explicit, with complex boundaries being readily handled. One of the major requirements is that the underlying discrete symmetry of the chosen lattice not mar the intended physics emulating from the continuously symmetric macroscopic equations. Initially, the spatial and (phase space) velocity lattices were intrinsically coupled and, because of the need to be space filling, this restricted the lattice geometry in 2D to be either a composite square grid or a hexagonal grid (with sufficient number of propagation speeds) or the projection of a 4D face-centered hypercube (FCHC) into 3D [7]. Recently, nonuniform

spatial grids have been introduced to more accurately handle wall-bounded flows [8]. This, as well as the recent use of finite difference schemes [9], allows for the decoupling of the spatial grid from the velocity lattice. However, it does not seem to have been appreciated that this decoupling now frees us to employ higher order symmetric velocity lattices which result in impressive gains in stability. Indeed, here we shall examine some of the consequences of employing an octagonal velocity lattice in 2D and its generalizations to 3D.

We shall utilize a Lagrangian free-streaming algorithm but, of course, our ideas are immediately applicable to any other scheme (finite difference, finite volume, etc.). On a particularly chosen discrete lattice, the kinetic equation (in lattice units) takes the form

$$N_{pi}(\mathbf{x} + \mathbf{c}_{pi}, t + 1) - N_{pi}(\mathbf{x}, t) = \Omega_{pi}(\mathbf{x}, t), \quad (1)$$

$$i = 1, \dots, b_p, \quad p = 1, \dots, S,$$

where \mathbf{c}_{pi} is the lattice velocity vector with free streaming in direction i at speed $|\mathbf{c}_{pi}|$. b_p is the number of links at speed index p , S is the total number of speeds in the model, and N_B is the total number of base vectors (or “bits”): $N_B = \sum b_p$. For lattice gas [1], N_{pi} is an integer representing the particle occupation number on site \mathbf{x} at time t for momentum state (pi) while, for lattice Boltzmann [2], N_{pi} is a (continuous) particle distribution function. The collision operator Ω_{pi} is constrained to satisfy (at each spatial node) particle, momentum, and energy conservation

$$\sum_{pi} \Omega_{pi}(\mathbf{x}, t) = 0 = \sum_{pi} \Omega_{pi}(\mathbf{x}, t) \mathbf{c}_{pi}$$

$$= \frac{1}{2} \sum_{pi} \Omega_{pi}(\mathbf{x}, t) c_{pi}^2. \quad (2)$$

For variable Prandtl number flows, one must employ an extended [1,6] Bhatnagar-Gross-Krook (BGK) collision operator

$$\Omega_{pi} = -\frac{1}{\tau} \sum_j A_{ij} [N_{pj} - N_{pj}^{\text{eq}}],$$

$$A_{ij} = \delta_{ij} + \frac{\theta\tau}{b_p c_p^2} \mathbf{c}_{pi} \cdot \mathbf{c}_{pj}, \quad (3)$$

with A_{ij} being a circulant matrix and the relaxation rates τ and θ controlling the viscosity $\mu(\tau)$ and conductivity $\kappa(\tau, \theta)$ transport coefficients [1,2]. $\mu \rightarrow 0$ as $\tau \rightarrow 0.5+$.

The form of N^{eq} is critical. A local H theorem [10] can be shown for exponential (Maxwellian-like) N^{eq} , but, to enforce the nodal conservation quantities (2) and the moment definitions of mass, momentum, and internal energy,

$$\sum_{pi} N_{pi}^{\text{eq}} = \rho, \quad \sum_{pi} N_{pi}^{\text{eq}} \mathbf{c}_{pi} = \rho \mathbf{u},$$

$$\sum_{pi} N_{pi}^{\text{eq}} c_{pi\alpha} c_{pi\beta} = \frac{2}{D} \rho e \delta_{\alpha\beta} + \rho u_\alpha u_\beta, \quad (4)$$

exactly, one is forced into a polynomial representation:

$$N_{pi}^{\text{eq}} = \rho [A_p(e) + B_p(e) \mathbf{c}_{pi} \cdot \mathbf{u} + C_p(e) (\mathbf{c}_{pi} \cdot \mathbf{u})^2$$

$$+ D_p(e) u^2 + E_p(e) \mathbf{c}_{pi} \cdot \mathbf{u} u^2 + F_p(e) (\mathbf{c}_{pi} \cdot \mathbf{u})^3$$

$$+ G_p(e) (\mathbf{c}_{pi} \cdot \mathbf{u})^2 u^2 + H_p(e) u^4]. \quad (5)$$

The coefficients A_p, \dots, H_p are constrained by the level of isotropy in the chosen velocity lattice as well as satisfying (4) and those constraints needed to recover the macroscopic conservation equations in the long-time long-wavelength Chapman-Enskog limit:

$$\sum_{pi} N_{pi}^{\text{eq}} c_{pi\alpha} c_{pi\beta} c_{pi\gamma} = \frac{2}{D} \rho e (u_\alpha \delta_{\beta\gamma} + u_\beta \delta_{\gamma\alpha} + u_\gamma \delta_{\alpha\beta})$$

$$+ \rho u_\alpha u_\beta u_\gamma, \quad (6)$$

$$\sum_{pi} N_{pi}^{\text{eq}} c_{pi\alpha} c_{pi\beta} c_{pi}^2 = \frac{4(D+2)}{D^2} \rho e^2 \delta_{\alpha\beta} + \frac{2}{D} \rho e u^2 \delta_{\alpha\beta}$$

$$+ \frac{2(D+4)}{D} \rho e u_\alpha u_\beta + \rho u_\alpha u_\beta u^2 \quad (7)$$

(here D is the dimensionality of the spatial grid and summation over repeated subscripts is understood).

It is clear from (4)–(7), that the n th-lattice velocity moments

$$T_{\alpha, \dots, \zeta}^{(n)} \equiv \sum_p T_{p, \alpha, \dots, \zeta}^{(n)} \equiv \sum_p \sum_i c_{pi\alpha} \cdots c_{pi\zeta} \quad (8)$$

play a critical role. For arbitrary regular lattices, one finds

$$T_{p, \alpha\beta\gamma\delta}^{(4)} = \psi_p Y_{\alpha\beta\gamma\delta} + \phi_p (\delta_{\alpha\beta} \delta_{\gamma\delta} + \text{c.p.}),$$

$$T_{p, \alpha\beta\gamma\delta\epsilon\zeta}^{(6)} = \Psi_p Y_{\alpha\beta\gamma\delta\epsilon\zeta} + \Lambda_p (\delta_{\alpha\beta} Y_{\gamma\delta\epsilon\zeta} + \text{c.p.})$$

$$+ \Phi_p (\delta_{\alpha\beta} T_{\gamma\delta\epsilon\zeta}^{(4)} + \text{c.p.}), \quad (9)$$

where Y_{\dots} is the higher rank Kronecker tensor ($Y_{\dots} = 1$ if all indices are equal, 0 otherwise) and is anisotropic. ψ_p, \dots, Φ_p are coefficients determined explicitly once the lattice is specified and “c.p.” denotes cyclic permutation of indices. For example, consider the 2D TLBE 13-bit square lattice $\{p=1, i=1, \dots, 4; \mathbf{c}_{1i} = (\pm 1, 0), (0, \pm 1)\}$; $\{p=2, i=1, \dots, 4; \mathbf{c}_{2i} = (\pm 1, \pm 1)\}$; $\{p=3, i=1, \dots, 4; \mathbf{c}_{3i} = (\pm 2, 0), (0, \pm 2)\}$ and the rest particle $\{p=0, i=1; \mathbf{c}_{0i} = (0, 0)\}$. This lattice does not yield an isotropic fourth rank lattice tensor $T_p^{(4)}$ at any individual speed p , (9). To recover overall $T^{(4)}$ isotropy, (8), the minimal isotropy needed to recover the correct conservation equations (at least to leading order), further constraints (and speeds) must be enforced on the coefficients $A_p \dots$ of the relaxation distribution function, (5). These extra constraints have such strong adverse effects on the numerical stability (see Fig. 1) that this 2D TLBE 13-bit free-streaming square model is practically useless for our applications. It has been noted [11] that a 2D 17-bit square lattice can recover overall $T^{(6)}$ isotropy, but these models are even more numerically unstable due to the extra constraints placed on the expansion coefficients in (5).

The 2D 13-bit hexagonal lattice [3] does yield isotropic $T_p^{(4)}$ but not $T^{(6)}$ tensors. As a result, the hexagonal lattice exhibits better stability properties than the square lattice [12] (see Fig. 1), but it does not exhibit sufficient isotropy to eliminate the spurious cubic deviations in the macroscopic conservation equations [11]. Moreover [11], there does not seem to be a higher-bit hexagonal

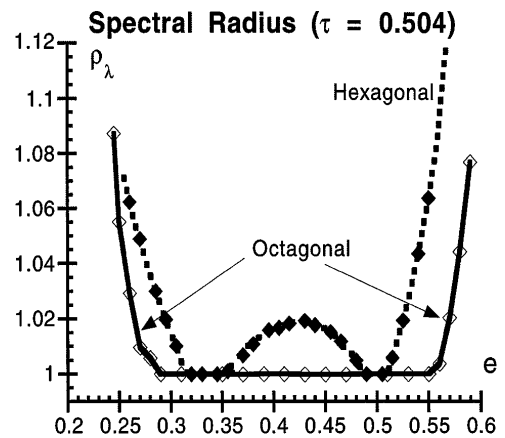


FIG. 1. Linear stability windows ($\rho_\lambda = 1$) for the octagonal grid, $0.28 < e < 0.555$, and the hexagonal grid, $0.32 < e < 0.505$ and $0.49 < e < 0.505$ for $\tau = 0.504$, and Prandtl number $\text{Pr} = \mu/\kappa = 0.5$ (i.e., $\theta = 0$). For this value of τ , there is no stable region for the 13-bit square grid, with $\min \rho_\lambda = 1.18$ ($\tau = 0.5$ corresponds to infinite Reynolds number).

lattice that will enforce $T^{(6)}$ isotropy. The reason so much emphasis has been placed on these 2D lattices is that they are space filling.

Since here we uncouple the velocity lattice from the spatial grid, the velocity lattice need no longer be space filling. Consider the 2D 17-bit octagonal model, with lattice vectors $[\mathbf{c}_{pi} = p(\cos \pi i/8, \sin \pi i/8), i = 0, \dots, 7, p = 1, 2]$ and rest particle. This octagonal lattice exhibits individual speed isotropy up to the sixth-rank lattice tensors $T_p^{(6)}$ [see Table I below and Eq. (9)] so that one can recover the thermal macroscopic equations exactly, without spurious cubic nonlinearities [11].

To proceed, we must now specify a spatial grid, and, for convenience, we consider the standard 17-bit square grid. If we free stream one time step using the octagonal velocities \mathbf{c}_{pi} , only those directions with i even will fall on a spatial square node. In the diagonal directions (i odd), the spatial nodal radius = $2^{1/2}p$ while the octagonal free-streaming distance = p . Thus we must resort to some interpolation schemes to latch onto the chosen spatial grid nodes. The numerical stability [12] of this 2D octagonal TLBE model is shown in Fig. 1 for relaxation times $\tau = 0.504$ and $\theta = 0$ (i.e., for the standard BGK collision term. Previous numerical tests on the 2D hexagonal lattice have shown that the stability is independent of the Prandtl numbers $Pr = \mu/\kappa$ for $Pr > 0.03$). Note that the 2D 13-bit square lattice has no stability window in the internal energy e for any $\tau < 0.58$. The hexagonal lattice has limited disjoint stability windows $0.32 < e < 0.35$ and $0.49 < e < 0.505$ for $\tau = 0.504$, while the 2D octagonal mode has an extensive continuous stability window $0.28 < e < 0.555$.

Here we have employed a second order interpolation scheme for the diagonal directions (i odd). It is important to ascertain the effect of interpolation on the transport coefficients—especially since interpolation will always be needed in Lagrangian schemes on uncoupled lattices. Performing the standard [3] isothermal plane Poiseuille flow determination of the viscosity and the Fourier heat flux law for the conductivity, we find excellent agreement between theoretical Chapman-Enskog transport and that determined from our interpolated octagonal TLBE simulation, Figs. 2 and 3. (A standard bounce-back scheme is employed at the boundaries.)

The temperature profile in 2D Rayleigh-Benard convection is presented in Fig. 4 at times $t = 5$ K and $t =$

TABLE I. Individual speed isotropy of the octagonal lattice.

Octagonal grid (17-bit)	ψ_p	ϕ_p	Ψ_p	Λ_p	Φ_p
$p = 1$					
Speed-1	0	1	0	0	$\frac{1}{6}$
$p = 2$					
Speed-2	0	16	0	0	$\frac{3}{32}$

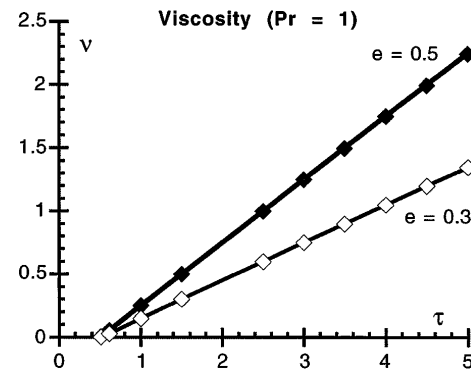


FIG. 2. Comparison of the theoretical Chapman-Enskog viscosity ν_{TH} (solid lines) to the 17-bit octagonal TLBE simulation viscosity ν_{SIM} (filled squares for $e = 0.5$, and open squares for $e = 0.3$) as a function of τ at $Pr = 1$ for isothermal plane Poiseuille flow. We have verified that ν_{SIM} is independent of the Prandtl number and find excellent agreement with ν_{TH} : e.g., for $e = 0.5$ and $Pr = 1$, $\nu_{TH} = -0.25 + 0.5\tau$, while $\nu_{SIM} = -0.249 + 0.499\tau$.

200 K lattice units. The lower plate ($y = 0$) is at internal energy $e = 0.5$, while the upper plate ($y = 129$) is at $e = 0.3$. The gravitational force $\rho\mathbf{G}$ is the $-y$ direction and is readily incorporated into the collision operator, Eq. (3), by the addition [11] of a term proportional to \mathbf{c}_{pi} . The Rayleigh number Ra , a ratio of the buoyancy to diffusion, for this run was 6×10^6 . A weak period-4 perturbation in the x direction was initially imposed on a straight line conduction profile. After 5 K iterations, Fig. 4(a), four strong convection cells are evident. At this high Rayleigh number, the flow is turbulent. By $t > 30$ K, turbulent effects are evident [c.f., Fig. 4(b)].

Finally, we have performed some preliminary stability tests on our extended 3D “octagonal” 53-bit TLBE model and compared them to that for the standard 4D FCHC-projected 34-bit model in 3D. For $\tau = 0.52$, the standard FCHC-projected model has no stability window in

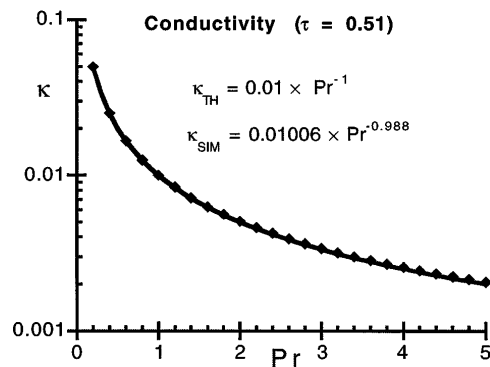


FIG. 3. The dependence of the conductivity on the Prandtl number at $\tau = 0.51$. Again, excellent agreement is found between the theoretical Chapman-Enskog conductivity κ_{TH} (solid curve) and that from the 17-bit TLBE octagonal simulation (solid diamonds).

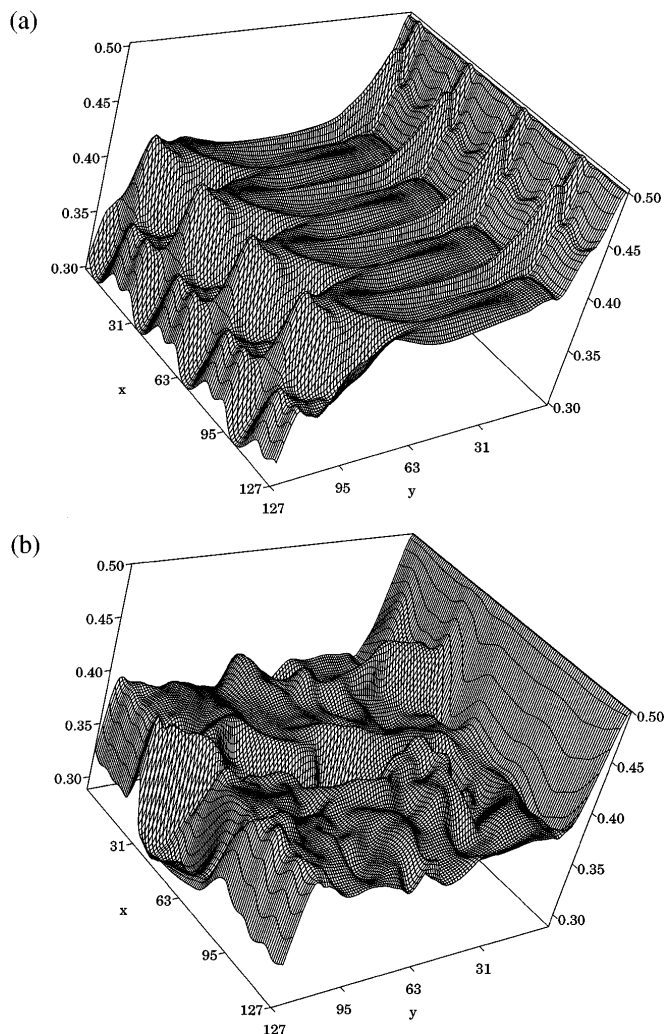


FIG. 4. Temperature profiles for 2D Rayleigh-Benard convection. The lower plate ($y = 0$) is at temperature $e = 0.5$ while the upper plate ($y = 129$) is at $e = 0.3$. The Rayleigh number $Ra = 6.0 \times 10^6$. After a short time, the convection patterns [(a) $t = 5$ K] become turbulent [(b) $t = 200$ K].

energy e , while our 53-bit model has an extensive stable region $0.28 < e < 0.72$. Thus, not only do we have a much greater stability window in e , but our model can enforce $T^{(6)}$ isotropic—while the FCHC model has only $T^{(4)}$ isotropy. More details of our 3D model will be presented elsewhere.

This work was supported by a joint U.S.-Czech grant and DOE.

*Also at Institute for Computer Applications in Science and Engineering, NASA Langley Research Center, Hampton, Virginia 23665

- [1] H. Chen, C. Teixeira, and K. Molvig, *Int. J. Mod. Phys. C* **8**, 675 (1997).
- [2] S. Chen, S.P. Dawson, G.D. Doolen, D.R. Janecky, and A. Lawniczak, *Comput. Chem. Eng.* **19**, 617 (1995), and references therein.
- [3] F.J. Alexander, S. Chen, and J.D. Sterling, *Phys. Rev. E* **47**, R2249 (1993).
- [4] Y. Chen, H. Ohashi, and M. Akiyama, *Phys. Rev. E* **50**, 2276 (1994).
- [5] G.R. McNamara, A.L. Garcia, and B.J. Alder, *J. Stat. Phys.* **81**, 395 (1995).
- [6] G. Vahala, P. Pavlo, L. Vahala, and M. Soe, *Czech. J. Phys.* **46**, 1063 (1996).
- [7] U. Frisch, D. d'Humieres, B. Hasslacher, P. Lallemand, Y. Pomeau, and J.P. Rivet, *Complex Systems* **1**, 649 (1987); S. Wolfram, *J. Stat. Phys.* **45**, 471 (1986).
- [8] X. He, L.S. Luo, and M. Dembo, *J. Comput. Phys.* **129**, 357 (1996).
- [9] N. Cao, S. Chen, S. Jin, and D. Martinez, *Phys. Rev. E* **55**, R21 (1997).
- [10] M. Henon, *Complex Systems* **1**, 763 (1987); H. Chen, *J. Stat. Phys.* **81**, 347 (1995).
- [11] Y. Chen, Ph.D. thesis, University of Tokyo, 1994); Y.H. Qian and S.A. Orszag, *Europhys. Lett.* **21**, 255 (1993).
- [12] P. Pavlo, G. Vahala, L. Vahala, and M. Soe, *J. Comput. Phys.* **139**, 79 (1998).